12. P. S. Khuane, "Loss of strength in coarse porous bodies," Plast. Mass., No. 1 (1965).
13. M. Kats, "Modulus of elasticity of materials with a cellular-porous structure," Probl. Prochn., No. 3 (1972).
14. V. Herrman, "Equations of state for porous materials under compression," in: Problems in Structural Strength Theory, 7th Ed. [Russian translation], Mir, Moscow (1976).
15. J. R. Asay, "Shock and release behavior in porous 1100 aluminum," J. Appl. Phys., 46, No. 11 (1975).
16. R. R. Boade, "Dynamic compression of porous tungsten," J. Appl. Phys., 40, No. 9 (1969).
17. D. R. Dundekar and R. M. Lamothe, "Behavior of porous tungsten under shock compression at room temperature," J. Appl. Phys., 48, No. 7 (1977).
18. A. Buch and S. Goldschmidt, "Influence of porosity on elastic moduli of sintered materials," Mater. Sci. Engng., 4, No. 5 (1969/70).
19. G. Eden and C. R. Smith, "Elastic-plastic behavior of porous beryllium," in: Proc. 5th International Symposium on Detonation, Pasadena, California, 1970, Arlington (1970).
20. R. N. Schock, A. E. Aleg, and A. Duba, "Quasistatic deformation of porous beryllium and aluminum," J. Appl. Phys., 47, No. 1 (1976).
21. S. P. Marsh (ed.), LASL Shock Hugoniot data, Univ. California Press, Berkeley–Los Angeles–London (1980).
22. B. M. Butcher, M. M. Carroll, and A. C. Holt, "Shock wave compaction of porous aluminum," J. Appl. Phys., 45, No. 9 (1974).
23. B. M. Butcher, "Dynamic response of partially compacted porous aluminum during unloading," J. Appl. Phys., 44, No. 10 (1973).

MEASUREMENT OF HIGH ELECTRICAL CONDUCTIVITY IN SILICON IN SHOCK WAVES

S. D. Gilev and A. M. Trubachev

UDC 539.63:537.311.3

The study of dielectric (semiconductor)–metal phase transitions by measurement of electrical conductivity is of great interest in the physics of both shock waves and the solid state. The problem of conductivity measurement in a shock wave was formulated more than 20 years ago and has been considered by many authors [1-4]. The difficulties in solving this problem are related to the fact that under shock wave loading conditions the conductivity of the material changes by many orders of magnitude over a fraction of a microsecond, reaching values characteristic of classical metals. Measurement of conductivity under such conditions was considered in [5-11].

The most widely used measurement method is that involving a shunt connected in parallel with the specimen to be studied [5-9]. The shunt serves to couple the current to the power circuit and limits the range of change in voltage across the specimen. However, the spatial separation of the specimen and shunt leads to high inertia in the measurement circuit, which makes determination of high conductivity ($\sigma > 10^5\ \Omega^{-1}\cdot m^{-1}$) quite difficult. At present values in the range $\sigma \approx 10^4$-$10^5\ \Omega^{-1}\cdot m^{-1}$ can be recorded reliably.

The present study will offer an improved method for measurement of high conductivity together with a technique for processing the experimental data which insures nanosecond time resolution and raises the upper limit of measurable σ to 10^6-$10^7\ \Omega^{-1}\cdot m^{-1}$. The dependence of electrical conductivity on pressure will be determined for solid and porous silicon under conditions of single-time and multiple compression by shock waves in the intensity range 7-20 GPa.

1. Figure 1a shows the electrical circuit used for measurement of electrical conductivity during dielectric (semiconductor)–metal phase transitions. It includes a power supply (PS), shunt, and the specimen under study. At the initial moment the specimen resistance is high and practically all the current flows through the shunt. When the shock

Novosibirsk. Translated from Zhurnal Prikladnoi Mekhaniki i Tekhnicheskoi Fiziki, No. 6, pp. 61-67, November-December, 1988. Original article submitted September 23, 1987.

 0021-8944/88/2906-0818 $12.50

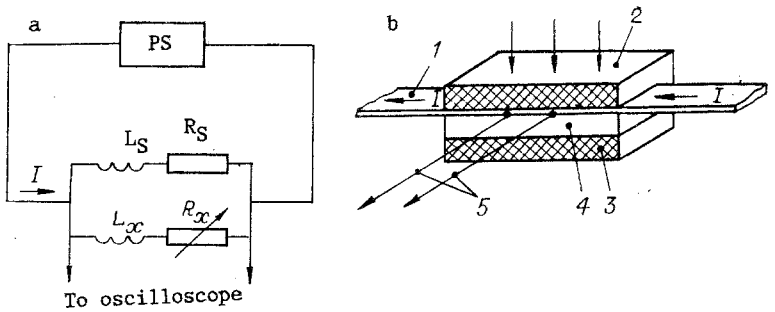

Fig. 1

wave impinges upon the specimen its resistance becomes comparable to the shunt resistance and the current I in the shunt-specimen circuit is redistributed over a characteristic time

$$\tau \sim (L_S + L_x)/(R_S + R_x). \tag{1.1}$$

where L_S, L_X, R_S, R_X are the inductance and resistance of the shunt and specimen. The quantity τ determines the time resolution of the circuit. When high conductivity is being measured the resistance of the measurement circuit is low but because of the spatial separation of the shunt and specimen its inductance remains high. This leads to large values of τ.

We will denote by τ_1 the period over which a high-pressure zone exists in the shock wave, while τ_2 will be the time required for shock wave passage through the specimen. Depending on the ratios of τ, τ_1, τ_2 three cases of practical importance are possible: for $\tau \gtrsim \tau_1$ correct measurement is impossible; for $\tau_2 < \tau \ll \tau_1$ it is possible, but only in a multiple compression mode, so that the state of the material is often poorly defined and the measurement result is a steady-state conductivity value with high uncertainty; for $\tau < \tau_2 \ll \tau_1$ conductivity measurements are possible for single time and multiple compressions. The above analysis is quite elementary, but the experiments found in the literature on high-conductivity measurements fall mainly into the first two cases as regards the characteristic time ratios.

It is clear from the above that decreasing the relaxation time is a most important problem, without solution of which one cannot hope to obtain reliable results on the conductivity of the material.

2. It is evident from Eq. (1.1) that to decrease the times of transient processes in the measurement network it is necessary to decrease its inductance. Figure 1b shows a diagram of a measurement cell with minimum inductance. The shunt 1, made of a thin flat foil, is placed upon the specimen 4 which has the same width, and is in electrical contact with the specimen over its entire surface. The layers 2, 3 are insulating material. A current is fed from a current generator through the leads of the shunt to the specimen and maintained constant during the measurement process. The shock wave enters the specimen through insulator 2 and shunt 1. The voltage across the specimen is taken from electrodes 5, located in the shunt–specimen contact plane perpendicular to the direction of current passage. Such construction significantly decreases the duration of the transient processes which limit time resolution and the measurable conductivity. A unique feature of the circuit is that measurements can be performed during the process of shock wave propagation under singlefold compression conditions. Measurements are also possible after arrival of the shock wave at insulator 3 and full establishment of the currents in the shunt–specimen circuit (multiple compression regime).

We will consider the process of shock wave propagation through the specimen. At t = 0 let the wave enter the material to be studied. We denote by D the shock wave front velocity, u is the mass velocity, h_1 is the thickness of the shunt, and h is the thickness of the specimen. Behind the shock wave front in the material a conductivity σ develops. As the shock wave propagates into the depths of the specimen the current from the shunt is redistributed through the layer of shock-compressed material.

We will make the following assumptions: 1) skin effect is absent in the shunt and specimen; 2) the specimen conductivity σ is constant over time; 3) the conductivity behind the shock wave front appears with no time delay; 4) the shunt resistance and total current in the circuit are constant. It is simple to show that with these assumptions the specimen conductivity can be found with the expression:

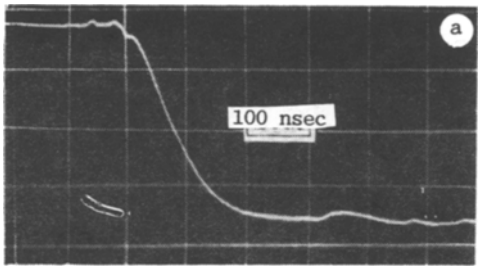

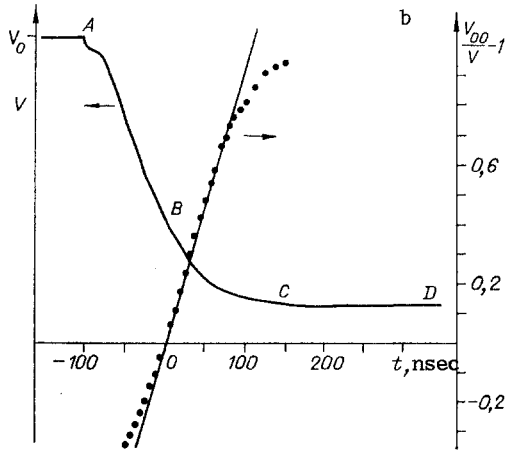

Fig. 2

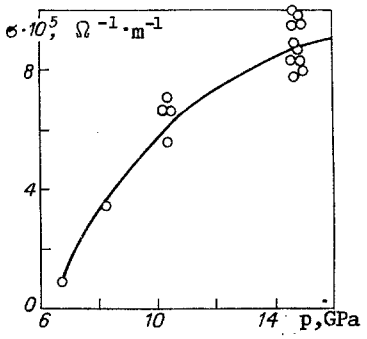

Fig. 3

$$\sigma = \frac{h_1\sigma_1}{D-u}\frac{1}{t}\left(\frac{V_0}{V(t)}-1\right), \quad 0<t<\frac{h}{D}. \tag{2.1}$$

Here V(t) is the voltage recorded across the electrodes; V_0 is the initial voltage; σ_1 is the conductivity of the shunt. The first two assumptions are of principal significance in the derivation of Eq. (2.1). A systematic deviation of the experimental dependence $\sigma = \sigma(t)$ obtained with Eq. (2.1) from constancy indicates the presence of a conductivity profile or the influence of skin effect. We will define the range of applicability of Eq. (2.1) with regard to skin effect. We write the condition for absence of skin effect up to the time t in the shunt

$$h_1 \ll \sqrt{t/(\mu_0\sigma_1)} \tag{2.2}$$

and in the specimen

$$(D-u)\,t \ll \sqrt{t/(\mu_0\sigma)}. \tag{2.3}$$

Simultaneous solution of Eqs. (2.2) and (2.3) gives the following limitations on the observation time:

$$\tau_3 \ll t \ll \tau_4. \tag{2.4}$$

Here $\tau_3 = h_1^2\mu_0\sigma_1$; $\tau^4 = [\mu_0\sigma(D-u)^2]^{-1}$ (τ_3 defines the skin effect in the shunt; τ_4, in the specimen). Condition (2.4) establishes the working range of Eq. (2.1) with respect to skin effect. Numerical estimates show that for measurement of high conductivity τ_3 and τ_4 lie in the nanosecond range.

We will also consider the question of time resolution of the proposed circuit. Generally speaking time resolution is determined by the skin effect in the shunt, $\tau = \tau_3$, and comprises units or tens of nanoseconds when thin foils are used. However, near t = 0 one must consider splitting of the incident shock wave in the shunt because of the differing shock impedances of the layers (insulator, shunt, specimen). The conductivity front resolution time τ_Φ is thus found to be the larger of two times: the shunt skin effect time τ_3 and the time for shock wave establishment in the shunt τ_5 : $\tau_\Phi = \max(\tau_3, \tau_5)$, where $\tau_5 \simeq h_1 n/c$ (c is the wave velocity in the front, n is the number of passages of the wave

TABLE 1

Material	Density 10^{-3} kg/m^3	a	λ	Reference
Copper	8,9	3,915	1,495	[12]
D16T	2,78	5,328	1,338	[13]
Hetinax	1,37	3,048	1,422	[13]
Porous silicon	1,0	0,173	1,84	[14]
Polystyrene	1,05	2,4	1,637	[15]

which insure equalization of pressure in the insulator and specimen). Estimates show that for use of a foil with $h_1 < 500$ μm $\tau_\phi = \tau_5$.

3. Experiments were performed to measure σ in porous and single-crystal silicon. The porous specimens were made from type KP-1 silicon, ground into a powder with particle diameters of about 1 μm, with specimen thickness of 0.8-3.5 mm. The single-crystal silicon used was in the form of a plate about 0.27 mm thick (initial resistivity ~100 Ω·cm). The current through the measurement cell was 500 A, maintained constant during the measurement process. The shunt was prepared from Constantin foil ~100 μm thick (shunt width 10 mm).

The measurement cell was loaded by a plane-wave generator 75 mm in diameter, which produced an approximately triangular pressure profile 5 μsec in duration. The generator insured planarity of the wave over 40 nsec at 50 mm diameter and for better than 10 nsec over the measurement lead base of 5-6 mm. Signals were recorded by an S1-75 oscilloscope with 250 MHz bandwidth.

The intensity of the incident shock wave was varied by using different explosives and buffer layers with different shock impedances. The pressure in the measurement cell was calculated from the known shock adiabats of the materials and monitored by a manganin sensor in a number of the experiments. The values of the coefficients in the expression $D = a + \lambda u$ are presented in Table 1 (data on shock compressibility of single-crystal silicon were taken from [16]).

Figure 2a shows an oscillogram from an experiment measuring conductivity of porous silicon. The shock wave brings the powder into a conductive state which is recorded in the oscillogram as a sharp drop in signal level. The incident shock wave undergoes splitting in the shunt, and a sequence of shock waves with increasing intensity exit into the silicon. The later waves have a higher propagation velocity and move through material which has already been compressed so that at some distance from the shunt within the specimen a single shock wave is again formed. The effect of wave splitting depends on the shunt thickness and leads to a characteristic inflection at the beginning of the oscillogram.

Figure 2b shows the same oscillogram and the result of its processing. The point A denotes the moment of shock wave arrival in the material, while C is the calculated time of shock wave exit into the insulating wall. The right-hand ordinate shows the dimensionless quantity $V_{00}/V - 1$ [V_{00} is the signal level taken as initial in the processing; the corresponding time is taken as zero (point B)]. For constant σ without skin effect, according to Eq. (2.1) this dependence should form a straight line. After shock wave establishment (~100 nsec) the experimental points fit a straight line fairly well, the slope of the line defining the electrical conductivity. The value found for σ by this processing comprises $8.9 \cdot 10^5$ $\Omega^{-1} \cdot m^{-1}$. Deviation of the points from the straight line at the first and last moments is related to skin effect.

Analysis of the experiments revealed that: 1) the manifestation of conductivity corresponded precisely to the moment of shock wave exit into the specimen, while if any delay did exist it was less than 5-10 nsec. Delay was determined by comparing the moment of shock wave exit into the specimen and the moment at which conductivity appeared; 2) the silicon conductivity in the compressed state remained practically constant over time; 3) the accuracy of σ determination with the given method of oscillogram processing was no worse than 10%. Since σ is determined from a large number of points in one and the same experiment, the method shows little sensitivity to spurious signals; 4) the measurement method permits tracing the qualitative dependence σ(p) in a single shot, because of shock wave splitting in the shunt. For porous silicon σ increases with increase in pressure p, as shown by the increase in slope of the oscillogram processing curve in its initial segment (the time interval AB in Fig. 2b).

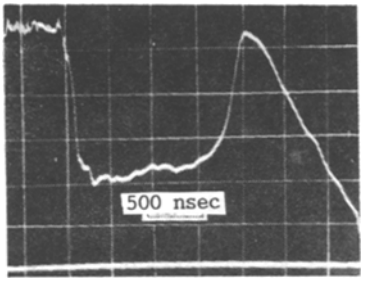

Fig. 4

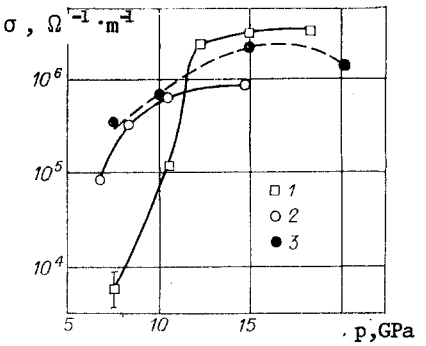

Fig. 5

Two shortcomings of the measurement cell should be noted: 1) since the initial segment of the oscillogram is excluded from examination, information on the dynamics of conductivity growth in the shock front is lost. The most radical method of improving the time resolution of the conductivity front is matching the impedances of the upper insulator and the shunt; 2) the specimen has a finite width and is surrounded by material with different shock wave properties. In the central portion the specimen is compressed by a planar shock wave, while at the edges its state is determined by a more complex interaction of waves. The dimension of the perturbed zone depends on the specimen thickness and the closeness of the shock adiabats of the materials. Estimates performed show that in the experiments conducted the contribution of edge effect to the measured σ value did not exceed 4% for the thickest specimens used, which lies within the limits of accuracy of the conductivity measurement method.

Figure 3 shows experimental results of measuring conductivity of porous silicon. Each circle corresponds to an individual experiment, in which the σ value was found by processing an oscillogram in the coordinates $(V_{00}/V - 1, t)$. The conductivity of the porous silicon increases with increase in pressure in the shock wave but traces of saturation can be seen in the function σ(p). The scattering of the points can be explained by scattering in the initial density of the porous silicon (±8%).

A series of single-crystal silicon experiments was performed with thin specimens so that the problem of tracing dynamics of the process was not considered and only the value of σ established after multiple wave passage was recorded. Otherwise the conduct of the experiments was the same as those with powdered silicon. The oscillogram of one such experiment is shown in Fig. 4. Under action of the shock wave the voltage across the measurement cell falls sharply. The slight further change in voltage is related to the falling pressure profile. After some time an unloading wave enters the specimen from its free surface and the silicon experiences a reverse transition to the nonconductive state (reverse transition time ~250 nsec). In the unloading wave the integrity of the electrical circuit is disrupted and the signal becomes unpredictable.

Measurements showed that upon removal of p in the unloading wave the single-crystal shows significant hysteresis in its conductivity, reaching more than an order of magnitude. Hysteresis also occurs for porous silicon, although due to the smoother dependence of σ on p and indefiniteness in the position of the unloading isoentrope it is more difficult to record reliably.

Figure 5 shows results of σ measurements in single-crystal silicon 1 together with averaged results for powdered silicon 2. Comparison of the experimental results shows that for $p < 12$ GPa the function σ(p) for the single-crystal is significantly more intense than for the powder, and has a plateau character for high p. As is well known, at high pressure silicon experiences a semiconductor–metal phase transition [17, 18]. This is a polymorphic transition, characterized by a change in the crystalline lattice structure from a cubic diamond type to a white tin type lattice. The pressure for this phase transition, as determined in [16] from the cusp in the shock adiabat, is 13.4 GPa. The total increase in σ in the shock wave in the present experiments was 10^6 times for the solid silicon and more than 10^{12} times for the porous.

Figure 5 also shows results of σ measurements in porous silicon under multiple compression conditions 3. The silicon powder was located in a narrow gap between hetinax plates. The σ calculation was performed for the settled voltage level (marker D of Fig.

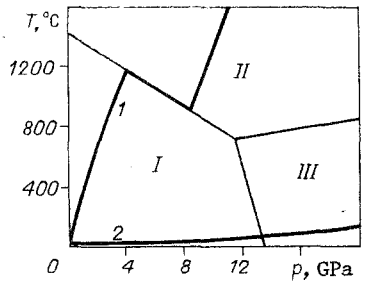

Fig. 6

2b). On the average the points for multiple compression lie above those for single compression, although measurements under such conditions have intrinsically higher uncertainty, related to indefiniteness in the position of the shock adiabat for multiple compression and the low final signal level. Nevertheless comparison of the data on compression of porous silicon shows that reduction in temperature of the shock-compressed material leads to an increase in σ, indicating its metallic character.

In the variables T–p Fig. 6 shows the phase diagram of silicon [19] and calculated functions T–T(p) for porous (1) and solid (2) silicon during compression by a shock wave. In regions I-III the silicon exists as a semiconductor, a fused phase, and a metallic phase (the melted phase shows metallic properties). Of interest is the fact that although the conductivities of solid and porous silicon are similar in order of magnitude in the phase transition region the mechanisms whereby conduction appears differ significantly. The conductivity of porous silicon increases because of its fusion in the shock wave. It is characteristic that the σ values obtained are close to the conductivity of the melt at atmospheric pressure [20]. The conductivity of solid silicon appears during the process of the semiconductor–metal phase transition with pressure playing the fundamental role. Therefore the function $\sigma(p)$ for solid silicon in the pressure range before the phase transition has a higher slope.

4. The method of processing the experimental data considered above assumes the absence of skin effect in the shunt and specimen. To study the limiting capabilities of the method the one-dimensional problem of skin effect in the shunt–specimen system was considered. The problem was solved numerically, and the specimen conductivity behind the shock wave front was assumed constant. Solutions were obtained for moments corresponding to shock wave propagation through the specimen (singlefold compression regime) and for times after the arrival of the shock wave on the wall and complete settling of the currents (multiple compression regime). During the course of the solution parameters of the shunt–specimen system were found for which skin effect was low. Estimates of the limiting conductivity for the single compression regime yielded $4\cdot10^5$ $\Omega^{-1}\cdot m^{-1}$ for low compressibility metal-type materials and 10^6 $\Omega^{-1}\cdot m^{-1}$ for materials with u/D = 0.5. The multiple compression regime permits a significant increase in the upper limit of measurable conductivity: 10^7 $\Omega^{-1}\cdot m^{-1}$ for low compressibility material and $3\cdot10^7$ $\Omega^{-1}\cdot m^{-1}$ for materials with u/D = 0.5. The analysis performed shows that it is possible to perform σ measurements in a shock wave corresponding to the conductivity of conventional metals. To a significant extent the proposed method solves the old problem of measurement of high conductivity of material during dielectric–metal phase transitions in a shock wave.

The authors are indebted to E. I. Bichenkov for advice and support in completing the study.

LITERATURE CITED

1. B. Alder, "Physical experiments with strong shock waves," in: Solid Bodies under High Pressure [Russian translation], Mir, Moscow (1966).
2. D. L. Styris and G. E. Duvall, "Electrical conductivity of materials under shock compression," High Temp.-High Pres., 2, No. 5 (1970).
3. R. Kyler, "Electrical conductivity of condensed media under high pressures," in: Physics of High Energy Densities [Russian translation], Mir, Moscow (1974).
4. V. V. Yakushev, "Electrical measurements in dynamic experiment," Fiz. Goreniya Vzryva, No. 2 (1978).
5. L. V. Kuleshova, "Electrical conductivity of boron nitride, potassium chloride, and Teflon-4 behind shock wave fronts," Fiz. Tverd. Tela, 11, No. 5 (1969).

6. S. S. Nabatov, A. N. Dremin, et al., "Change in electrical conductivity of sulfur upon dynamic loading to 400 kbar," Zh. Tekh. Fiz., 5, No. 3 (1979).
7. S. S. Nabatov, A. N. Dremin, et al., "Measurement of electrical conductivity of sulfur at superhigh dynamic pressures," Pis'ma Zh. Éksp. Teor. Fiz., 29, No. 7 (1979).
8. V. I. Postnov, L. A. Anan'eva, et al., "Electrical conductivity and compressibility of sulfur under shock compression," Fiz. Goreniya Vzryva, No. 4 (1986).
9. T. Mashimo, Y. Kimura, and K. Nagayama, Precise Measurement of the Electrical Conductivity of Silicon under Shock Compression, Kumamoto Univ. (1984).
10. L. A. Gatilov and L. V. Kuleshova, "Measurement of high electrical conductivity in shock-compressed dielectrics," Zh. Prikl. Mekh. Tekh. Fiz., No. 1 (1981).
11. L. A. Gatilov and L. V. Kuleshova, "Electrical conductivity of cesium iodide behind a shock wave front at pressures to 100 GPa," Fiz. Tverd. Tela, 23, No. 9 (1981).
12. L. V. Al'tshuler, A. A. Bakanova, et al., "Shock adiabats of metals. New data, statistical analyses, and general principles," Zh. Prikl. Mekh. Tekh. Fiz., No. 2 (1981).
13. K. P. Stanyukovich (ed.), Explosion Physics [in Russian], Nauka, Moscow (1975).
14. K. Nagayama and T. Mashimo, "Magnetohydrodynamic study of flux cumulation by the propagation of shock-compressed conductive region in semiconductors," in: Superstrong Magnetic Fields. Physics. Technology. Application [in Russian], Nauka, Moscow (1984).
15. M. van Thiel (ed.), Compendium of Shock Wave Data, Livermore (1966).
16. T. Goto, T. Sato, and Y. Syono, "Reduction of shear strength and phase-transition in shock-loaded silicon," Jpn. J. Appl. Phys., 21, No. 6 (1982).
17. F. P. Bundy, "Phase diagrams of silicon and germanium to 200 kbar, 1000°C," J. Chem. Phys., 41, No. 12 (1964).
18. M. N. Pavlovskii, "Formation of metallic modifications of germanium and silicon under shock compression conditions," Fiz. Tverd. Tela, 9, No. 11 (1967).
19. E. Yu. Tonkov, Phase Diagrams of the Elements at High Pressure [in Russian], Nauka, Moscow (1979).
20. V. M. Glazov, S. N. Chizhevskaya, and N. N. Glagoleva, Liquid Semiconductors [in Russian], Nauka, Moscow (1967).

VISCOELASTICITY OF ALUMINUM IN RAREFACTION WAVES

G. I. Kanel', S. V. Razorenov, and V. E. Formov

UDC 532.593

It has been shown previously [1-3] that in shock-compressed metals both loading compression waves and rarefaction waves have elastic precursors. Analysis of the change of state in compression and rarefaction waves following a shock wave has shown that increments in deviator stresses in these waves can significantly exceed the stress anisotropy behind the shock wave front. Such a situation does not agree with simple models of an elastoplastic body, according to which increments in deformation in the plastic region are related to insignificant or even zero increments in deviator stresses, while the corresponding rate of propagation of weak loading waves is close to the "volume" speed of sound $c_b = (\partial p/\partial \rho)_s^{1/2}$. Such features of stress-deformed states and their changes behind a shock wave in metals have been explained by stress relaxation processes [1, 4, 5] or the specifics of high-speed metal deformation in the shock wave [3], involving heating of slip planes which leads to significant short-term loss of shear strength in the metal. In the latter cases resistance to deformation is reestablished as temperatures equalize behind the shock wave front and is practically independent of deformation rate.

In a Maxwell-type elastoviscous medium after the specimen is maintained at a fixed deformation, independent of their sign weak perturbations should propagate like purely elastic waves with a velocity $c_l = \sqrt{(K + (4/3)\,G)/\rho}$. In particular, for a steplike rarefaction the speed of the loading wave front should be equal to c_l. If the processes of

Chernogolovka. Translated from Zhurnal Prikladnoi Mekhaniki i Tekhnicheskoi Fiziki, No. 6, pp. 67-70, November-December, 1988. Original article submitted September 23, 1987.

 0021-8944/88/2906-0824 $12.50